ANALYSIS OF A GROUND BASED SYSTEM
FOR THE CALIBRATION OF ORBITAL UV TELESCOPES
WITH PIXELATED DETECTORS

E. M. POPESCU[1], A. A. RADU[1], M. HAIDUC[1], E. FIRU[1], A.T. NEAGU[1]

[1]Institute of Space Science, 409 Atomistilor Street, Magurele, Romania,
E-mails: empopescu@spacescience.ro; aurelian.radu@spacescience.ro

Abstract. In this paper we present a study of a ground-based calibration system for orbital UV telescopes used in the detection of EASs. The study is performed using a custom developed software package, GBSatCal, and as a result we propose a novel light source for the calibration system as well as the possibility of optimizing the calibration procedure.

Key words: calibration, TUS, JEM-EUSO, EAS, UHECR, UV telescope, pixelated detector.

1. INTRODUCTION

One of the major issues of the operation of the TUS [1], KLYPVE [2] and JEM-EUSO [3] missions – all three being essentially orbital telescopes for the detection of the UV and Cherenkov yield of extended air showers (EAS) generated by extragalactic ultra-high energy cosmic rays (UHECR) – is the calibration of the radiation detector. Noting that the detectors of all the instruments mentioned above are pixelated detectors, at the present time there are two distinct approaches for their calibration, namely (a) by using UV calibrated radiation sources (essentially low power UV LEDs) which are integrated in the construction of the orbital telescope and (b) by using ground calibrated UV radiation sources to illuminate the detector according to a pre-defined calibration schedule depending mainly on the particularities of the host satellite orbit.

The latter approach, which is the main focus of the present work, represents essentially the extension to spaceborne instruments of the technique used by the Central Laser Facility (CLF) [4] of the Pierre Auger Observatory (PAO) [5]. In brief, the CLF uses a combination of nanosecond pulsed ground UV lasers and airborne UV LEDs to illuminate the ground UV telescopes of the experiment. As these UV sources have carefully measured optical power outputs, with a careful monitoring of the weather conditions over the area covered by the UV telescopes, the latter can be reliably calibrated by either direct illumination (airborne LEDs) or indirect illumination (ground lasers).

However, while this approach has been successful for the calibration of ground UV telescopes and is currently in use at the PAO experiment, its extension to orbital UV telescopes is by no means straightforward. The easiest way to understand this issue is to note that as UHECR generated EASs have maxima at altitudes ranging from about 40 km to about 100 km depending on the type of primary particle, orbital UV telescopes observe these showers from a distance which is up to an order of magnitude larger than the observation distance of ground telescopes. This difference in observation distance, however, must not be thought of solely in terms of geometrical optics (*e.g.* magnification, resolving power, etc.), but also in terms of the "amount of atmosphere" involved in the observation. Indeed, while the observation of EASs by ground telescopes involves mainly what is known as the Earth's homosphere (*i.e.* the part of the atmosphere with an altitude ranging from the surface to about 100 km) [6], the orbital observation of EASs involves the entire Earth's atmosphere, from essentially the surface up to 500 km in the exosphere (about 350 km for the JEM-EUSO and KLYPVE missions on the International Space Station and about 450–500 km for the TUS mission).

Under these circumstances, while the basic idea of a ground calibration system is the same for both ground and orbital telescopes, for the latter case the calibration system must be redesigned to account for the entire atmosphere between the EAS and the observation point, and re-evaluated accordingly. This is exactly what the present study proposes to do by using a custom software package called the Ground-Based Satellite Calibration (GBSatCal) package, which has been developed by the authors specifically for this purpose.

The paper is organized as follows. In Section 2 we will give a brief review of the GBSatCal package and of its performance. In Section 3, we will present the results of our study, with emphasis on the operational parameters of the calibration system light sources and on the optimal calibration geometry. The paper will be concluded in Section 4 with a brief summary of our results and with plans for future work.

2. THE GBSatCal SIMULATION SOFTWARE PACKAGE

2.1. THE GBSatCal SIMULATION GEOMETRY

For reasons of simplicity, in the present study we have used the geometrical setup of the TUS mission, as illustrated in Fig. 1. In this setup, and in accordance with the TUS mission operational parameters, the satellite housing the telescope (the Lomonosov satellite) will be circling the Earth on a heliosynchronous orbit with an average altitude of $H = 500$ km from the Earth's surface. The telescope itself consists of a 1.6 m^2 Fresnel mirror with a 1.5 m focal distance, and of a 16×16 pixels detector made out of 256 Hamamatsu R1463 photomultiplier tubes (PMTs) [7] with a maximum of their spectral sensitivity in the near UV around the

wavelength $\lambda = 380$ nm. The telescope is pointing at nadir, and has a symmetric field of view (FoV) spanning an angle of $\beta = 9°$. In particular, this means that the telescope's FoV spans on the Earth's surface an area of about 80×80 km^2, corresponding to an average area of 5×5 km^2 for each pixel, or equivalently to a $0.56°$ FoV angle for each pixel.
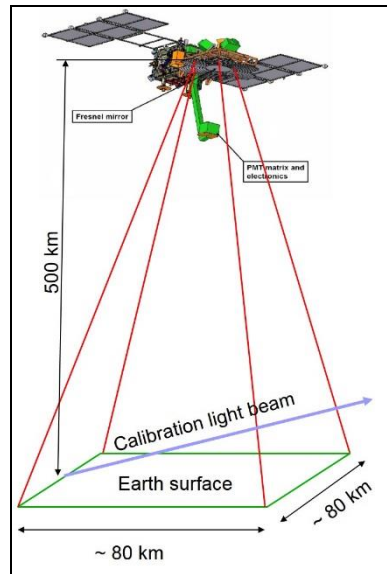
Fig. 1 – Ground calibration geometry for the TUS telescope.

Under these circumstances, we have considered an idealized calibration configuration consisting of a UV light source placed exactly on the boundary of the telescope's FoV, which shoots a pulsed parallel beam of light at an angle δ with respect at the local horizontal. As the light beam propagates through the atmosphere, its photons will be scattered away by the interaction with the molecular constituents of the former and part of them will reach the telescope's detector pixels after further propagation and scattering. This is in a nutshell the calibration phenomenology.

In the GBSatCal code, the light beam parameters, namely the angle δ, the intensity at the source I_0, the wavelength λ, the pulse duration $\Delta\tau$ and the pulse repetition rate ν are user settable, and can be varied from one simulation run to the next. In accordance with the TUS telescope operational characteristics, in all our simulation runs we have used for the pulse duration a value $\Delta\tau = 30$ μs, for the pulse repetition rate a value of $\nu = 1$ kHz, and for the wavelength a value of $\lambda = 365$ nm. The reason for the latter choice will become clear shortly.

Furthermore, as a pixel spans a 5×5 km^2 area on the Earth's surface, we have assumed that the focal plane pixelated detector of the telescope is oriented such that all the rows of 16 pixels are parallel with the projection of the calibration light

beam on the local horizontal, and that there is one row of 16 pixels which is in the same local vertical plane as the light beam and is illuminated by it. In this way, we have reduced without any loss of generality a 3-dimensional problem to a 2-dimensional one, which is much easier to code and to solve. For further reference, we have labelled as Pixel 1 the pixel in the illuminated row which is the closest to the light source, and as Pixel 16 the pixel in the illuminated row which is the farthest from the light source.

2.2. THE GBSatCal ATMOSPHERE MODEL

As mentioned in Section 2.1, the calibration method under discussion relies essentially on the scattering of the calibration light beam photons by the molecular constituents of the atmosphere. As such, it is necessary for the simulation software to include a model of the atmosphere which is appropriate for the task at hand.

For a variety of purposes, and not in the least for the design of space missions, starting with the late 1940s and early 1950s, several models of the atmosphere have been developed. These models have been continuously improved and changed, following essentially the trend of the atmospheric probing, monitoring and characterization technologies. At the present time, there are several choices of such models that have gained worldwide acceptance and recognition, such as the 1976 US Atmosphere Standard (USAS) model [8], the 2012 and 1986 COSPAR International Reference Atmosphere (CIRA) models [6, 9], the 2000 Naval Research Laboratory Mass Spectrometer Incoherent Scatter Radar Extended Model (NRLMSISE00) [10] and the US 2010 Earth General Reference Atmosphere Model (EarthGRAM) [11]. However, in order to comply with the accepted custom in the field (*e.g.* in the ESAF software package [12] for the JEM-EUSO mission) and to allow for the independent verification and validation of our data, we have decided to implement in the GBSatCal code the 1976 USAS model of the atmosphere.

According to this model, which covers altitudes ranging from the Earth's surface up to 1000 km, the atmosphere consists of 12 separate layers, each layer being characterized by a specific temperature variation with altitude. The temperature-altitude profiles are analytic, depending on standardized constants and the atmosphere is considered an ideal gas in steady-state equilibrium. As such, below 86 km the atmosphere is considered to be well mixed (wind-dominated region) and having a composition which is independent of location and altitude, hence yielding for the total number density of the atmosphere required by the simulation analytical formulae. Above 86 km however, due to significant diffusive separation of the atmospheric molecular species (diffusion dominated region), the composition of the atmosphere varies with altitude and the total number density of the atmosphere can only be calculated numerically.

Under these circumstances, in order to increase the computational speed of the GBSatCal software, we have decided to introduce for altitudes above 86 km additional computational layers and to fit the profile in each layer with a 10 degree polynomial function. In this way, for the entire altitude range from 0 km to 500 km – the average orbital altitude of the Lomonosov satellite carrying the TUS telescope – we have used a total number of 24 computational layers instead of the 17 required by the original model recommendations, with the former number being determined by the requirement that the fitted profile above 86 km be in each of the layers comparable or below the computational errors of the profile calculated by us according to the recommendations in the 1976 USAS model. The error analysis summary is presented in Fig. 2 below.
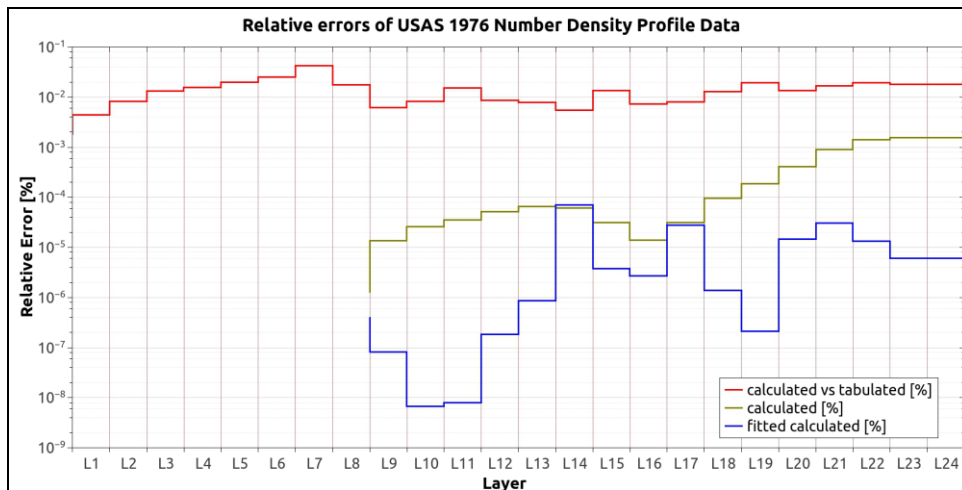
Fig. 2 – Comparative unsigned errors for the method of calculating the total number density
in the range 0–500 km implemented in the GBSatCal software.

The highest segmented line in Fig. 2 (red) represents the plot of the average relative unsigned error (*i.e.* the absolute value of the relative error) per layer between the 1076 USAS tabulated total number density profile and the total number density profile calculated by us according to the model recommendations. As it can be seen, over the entire altitude range spanned by the 24 computational layers, the error is below 0.1%, which is more than enough for our purposes. It should be noted that below 86 km, *i.e.* in the layers L1-L8, as the total number density is represented by analytic formulae, these errors are due simply to the difference in precision between the tabulated numerical values and our numerical values.

Above 86 km, *i.e.* in the L9-L24 layers, as mentioned earlier, the number density can only be calculated numerically, and the expressions that require

numerical evaluation contain integrals of functions depending solely on the altitude. As such, in order to be able to evaluate the computational errors, we have used a highly refined partition/meshing of the altitude range (essentially we have calculated the total number density in steps of 5 cm) and we have calculated the expressions by approximating the integrals with lower and respectively upper Riemann sums. The value of the number density at each point was taken as the average of the resulting lower and upper Riemann summed total number density values, and the relative errors per point were calculated using the ratio of their difference to the average value. The average errors per layer were calculated in the usual way, and are represented in Fig. 2 by the middle segmented line (green). It is clear from this data that our method for calculating the total number density in each layer above 86 km introduces unsigned errors which are by at least one order of magnitude smaller in each layer than the unsigned errors between the calculated and tabulated total number densities, *i.e.* that our lower/upper Riemann sum computational method introduces negligible errors compared to the tabulated values of the standard.

The lowest segmented line in Fig. 2 (blue) represents the relative errors (calculated in the usual way) on each layer of the fitted total number density with respect to the calculated total number density. The data confirms that the fitted total number density profile for each layer above 86 km is within the computational errors of the corresponding calculated total number density profile, as per the requirements stated earlier, and hence that the 24 computational layer model for the total number density in the altitude range from 0 km to 500 km is accurate enough to be implemented in the GBSatCal software.

2.3. THE GBSatCal EXTINCTION MODEL

As mentioned in Section 2.1, we have chosen for the wavelength of the calibration light source the value $\lambda = 365$ nm. The reason for this choice is that this wavelength is between the main fluorescence bands of the molecular nitrogen (N_2) in air centered at $\lambda = 358.21$ nm and $\lambda = 375.54$ nm, as well as between the much less intense fluorescence bands at $\lambda = 364.17$ nm and $\lambda = 367.19$ nm. Under these circumstances, during their propagation in the atmosphere, the photons in the calibration light beam will only be subjected to Rayleigh scattering, with no significant contribution due to absorption and emission/fluorescence phenomena, such that the scattering cross-section will be given by the classical expression [13]:

$$\sigma(\lambda) = \frac{24\pi^3}{\lambda^4 N^2} \left[\frac{n^2(\lambda)-1}{n^2(\lambda)+2} \right] F_K(\lambda), \tag{1}$$

where λ is the wavelength of the scattered radiation, N is the altitude dependent number density of the scattering species, $n(\lambda)$ is the wavelength dependent refractive index of the scattering species, and $F_K(\lambda)$ is the wavelength dependent

King factor (or depolarization factor) which accounts for the anisotropy of the scattering species molecule (*i.e.* for the anisotropy of the electric molecular polarizability.

In the 1976 USAS atmosphere model, the composition of the atmosphere is specified as a function of altitude. For altitudes below 86 km, it is independent of altitude and the volume fractions of the constitutive molecular species are fixed. Above 86 km, due to diffusive separation phenomena, the composition of the atmosphere varies with altitude and the volume fractions of the constitutive molecular species must be calculated using the recommendations of the model, or in our case, the 24 computational layers model in the regions of interest. Under these circumstances, and in the assumption of single scattering attenuation – i.e. that after being scattered once a photon in the beam is removed from the beam and never to re-enter due to subsequent scattering – the attenuation of the calibration light beam with the distance from the source will be given by a standard Beer-Lambert law having the form:

$$I(L) = I_0 e^{\left[-\Sigma_i \int_0^L N_i(t)\sigma_i(\lambda,t)dt\right]}, \tag{2}$$

where in the exponential the summation runs over all the atmospheric species contributing to the scattering of the photons in the light beam, the integral is calculated along the beam propagation path, $N_i(t)$ is the number density of the ith atmospheric species and $\sigma_i(\lambda,t)$ is the Rayleigh scattering cross-section given by eqn. (1). The latter two depend on the path length t essentially through the dependence on altitude of the number densities N_i of the atmospheric molecular species.
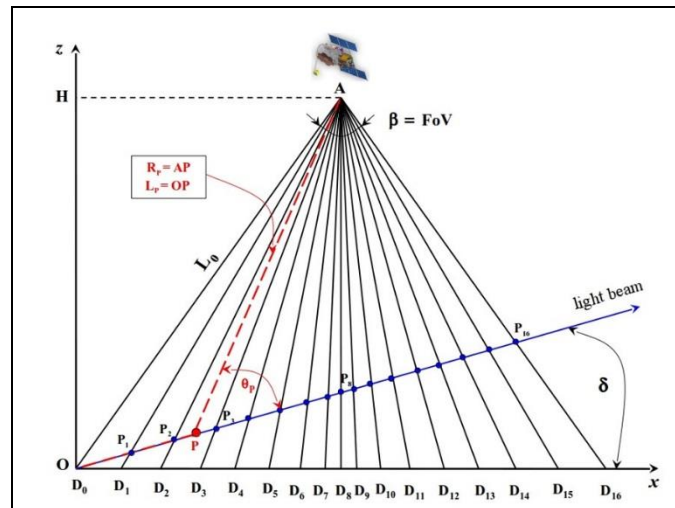
Fig. 3 – Illustration of the light propagation and attenuation methodology implemented in the GBSatCal software.

With these considerations, the GBSatCal implementation of the light propagation and attenuation algorithms for both the calibration beam as well as for the photons reaching the pixelated detector after being scattered away from the beam is illustrated in Fig. 3 below. The light beam originating at point O (the origin of the coordinate system) and propagating at an angle δ with respect to the local horizontal is divided by the FoV of the pixels in the detector's pixel row illuminated by the beam into segments $P_{i-1}P_i$, $i = 1, ... 16$. Each segment $P_{i-1}P_i$ will illuminate only the Pixel i, in the sense that in the assumption of single scattering attenuation, it is only the light scattered along this segment that is in the FoV of Pixel i and can reach it in orbit after subsequent scattering. Of course, the attenuation of the scattered light during its propagation from the segment $P_{i-1}P_i$ to Pixel i obeys an attenuation law similar to the one in eqn. (2).

In order to calculate the optical throughput of the segment $P_{i-1}P_i$ of the calibration beam to Pixel i, the GBSatCal software uses a straightforward discretization procedure. Each $P_{i-1}P_i$ segment of the calibration light beam is discretized in a user settable number j of smaller segments ΔP_j, and the total number of photons scattered by each ΔP_j segment is calculated using eqns. (2) and (3). In order to determine the number of photons reaching Pixel i from the segment ΔP_j, the algorithm implemented in GBSatCal makes use of the standard Rayleigh scattering phase function for each atmospheric species:

$$p_i(\theta_P) = \frac{3}{16\pi}\left[\frac{(2+\rho_i)+(1-2\rho_i)cos^2(\theta_P)}{(2+\rho_i)}\right],$$
(3)

where ρ_i is the depolarization coefficient of the i-th atmospheric species and θ_P is the angle of the line of sight from a point P representative of the segment $P_{i-1}P_i$ to the Pixel i of the detector. This phase function is integrated over the solid angle of the detector as seen from point P, and then multiplied by the total number of photons scattered by the segment ΔP_j of the calibration light beam to yield the number of photons that will start propagating towards Pixel i. Once again, in order to account for the scattering of these photons during their propagation to the pixel, we use eqns. (2) and (3) and a discretization method similar to the one just described. Finally, the total number of photons reaching the Pixel i from the calibration light beam segment $P_{i-1}P_i$ is obtained as the sum of the numbers of photons reaching the pixel from each sub-segment ΔP_j belonging to $P_{i-1}P_i$, and in this way the GBSatCal software determines the total number of photons reaching each of the 16 pixels in the pixel row of the detector.

It is extremely important to mention that the GBSatCal software is capable to provide for each pixel the errors in calculating the number of photons reaching it from the calibration light beam, in a manner similar to that described in Section 2.1. Indeed, all calculations involved in the propagation and attenuation of photons

in the calibration light beam and from the calibration light beam to the detector contain integrals that must be evaluated numerically. As such, for the calculation of these integrals we have implemented in the GBSatCal software algorithms that use lower and upper Riemann sums to provide in a consistent way a lower and an upper bound for the number of photons reaching each pixel, and have taken as representative the average of the two.

The above considerations conclude the present section as well as the discussion of the architecture and mathematical implementation of the GBSatCal software package.

3. RESULTS

As a first application of the GBSatCal software package, we have attempted to determine the functional parameters of the light sources that could be used on the ground for the calibration of the orbital TUS telescope detector. In order to do so, it is necessary to briefly discuss background illumination conditions under which the TUS telescope is supposed to operate.

In the satellite detection of EASs generated by UHECR – and regardless of whether we refer to the TUS, KLYPVE or JEM-EUSO missions – the major source of errors that limits not only the instrument detection performance but also its duty cycle is the UV radiation background [14]. This background, also called the night-time background, which can exceed by more than one order of magnitude the EAS signal received by the instrument and can have fluctuations at time scales that are comparable to EAS lifetimes, is mainly due to nightglow and to the reflection of solar radiation in the UV range on the Moon surface, and subsequently, to the reflection of this radiation from the Moon on the Earth's surface and on the various atmospheric layers. The most recent measurements of the atmospheric night-time background, are due to the Universitetsky Tatiana mission [15] which was launched in January 2005, and which lost contact in March 2007. According to their data, a reasonable value for the moonless night-time flux density is $\Phi_D \approx$ $\approx 3 \times 10^8 \pm 10\%$ ph$\times$cm$^{-2}\times$s$^{-1}\times$sr^{-1}, with fluctuations that can reach up to 20% of this value. For the purpose of calibrating the pixelated detector of the TUS telescope, it is the night-time background fluctuations that are of relevance, since in order to detect a calibration signal this signal has to be appropriately above the fluctuations level. Under these circumstances, the magnitude of the fluctuations can be considered as an ad-hoc threshold or standard deviation that must be exceeded by the calibration signal.

Referring now to the TUS telescope, with its particular geometry and operational characteristics described in the previous sections, for each pixel the night-time background fluctuations translate into a number $\sigma \approx 3500$ photons for each calibration pulse length $\Delta\tau = 30$ μs. This means that in order to be able to

unambiguously calibrate a pixel of the detector, the number of photons reaching the pixel for each calibration pulse must be at least 2σ, *i.e.* ~ 7000 photons during each 30 µs long calibration pulse.

With these numbers, we can now proceed with the analysis of the operational characteristics of the ground light sources that could be used to calibrate the TUS telescope in orbit. For this purpose, we have considered horizontal ($\delta = 0°$) calibration beams of different diameters, and with the rest of the simulation variables set as described in the previous sections, we have varied the source intensity and have determined the number of photons reaching each of the 16 pixels in the pixelated detector row. It should be noted that the set (intensity, beam diameter) can be used to distinguish between various possible light sources such as lasers, LEDs, etc. The results of our simulations are shown in Fig. 4.
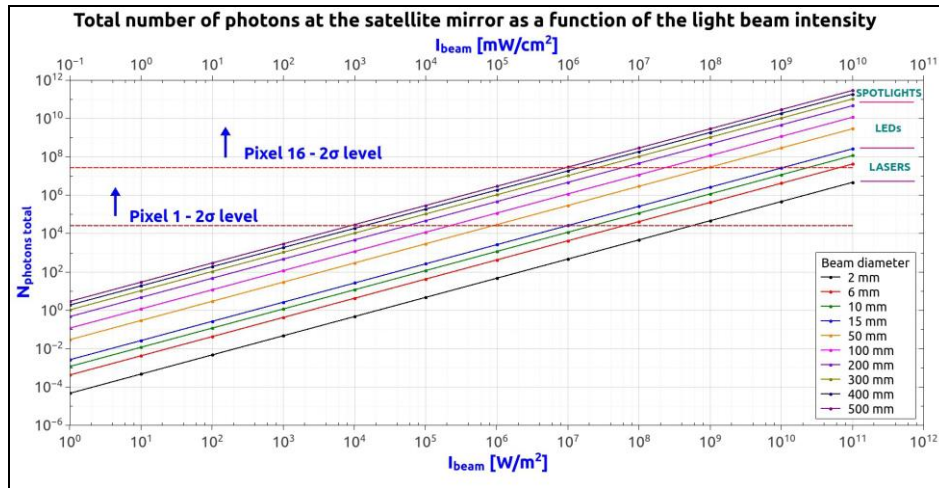
Fig. 4 – Simulation results for the analysis of the various ground light sources that could be used to calibrate in orbit the TUS telescope detector. Also shown are the 2σ levels for the calibration of just the first pixel (Pixel 1) in the row and for the calibration of all 16 pixels in the row.

It is clear from Fig. 4 that lasers can be successfully used to calibrate the pixels of the TUS telescope detector. For comparison purposes, the PAO Big Sky/Quantel YAG:Nd laser having a beam diameter of ~ 10 mm and an output intensity of 13×10^9 W/m^2 = 13×10^{10} mW/cm^2 could be used to calibrate at the 2σ level 10 of the 16 pixels in the detector's pixel rows. However, in order to calibrate all the pixels in the row, it is necessary to use more powerful and hence more expensive lasers than those used by the PAO and JEM-EUSO experiments.

A more interesting conclusion that can be drawn from Fig. 4 is related to the medium beam diameter light sources, *i.e.* to the light sources producing beams with diameters ranging from 50 mm to 200 mm. These light sources correspond to LED matrices (*i.e.* to a pixelated light source), consisting of high power or superbright

LED modules, such as the LZ1-00UV00 LED module from LEDEngin [16] which is 4.2×4.2 mm^2 in size and has an intensity of $1.4×10^5$ W/m^2 at $\lambda = 365$ nm. For comparison purposes, such a pixelated light source consisting of 10×10 LEDs would have an intensity of about $1.4×10^7$ W/m^2 and a beam size of about 50 mm, and according to Fig. 4, it could calibrate at the 2σ level 7–8 of the 16 pixels in the row. In other words, it would do the same job as the Big Sky/Quantel laser in use by the PAO experiment, but at only a fraction of the cost. To the best knowledge of the authors, they are the first to propose the use of such pixelated light sources for the in-orbit calibration of UV telescopes.

Of course, by examining the data for the large beam diameter light sources, corresponding essentially to spotlights, one can see that unless one can find light bulbs for them with a very high yield in UV, they are not exactly appropriate for the task at hand.

The conclusion of the above analysis is that while one could go ahead with the existing technology (*i.e.* with laser sources) to develop a ground system for the in-orbit calibration of UV telescopes, there is an alternative method, based on pixelated light sources with superbright LEDs that can do essentially the same job, bit which is much simpler technically and much more feasible from the economic viewpoint.

These being said, we can no proceed with the second part of our analysis, namely with the determination of an optimal calibration geometry. For this purpose, we have considered a 200 mm diameter calibration beam with a source intensity of 10^5 W/m^2 (corresponding to a 2σ level calibration of Pixel 1), we have set all the other simulation parameter values as before, and we have calculated the number of photons reaching the pixels as a function of the inclination angle δ. The results are presented in Fig. 5 below.
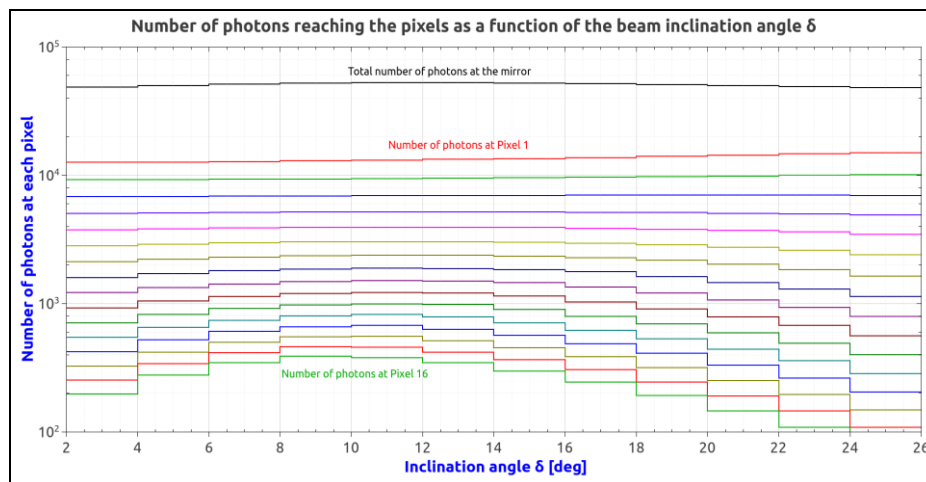
Fig. 5 – Influence of the inclination angle δ on the calibration efficiency.

By simple inspection of Fig. 5, it is clear that that there is an optimum angle $\delta \approx 12°$ for which the total number of photons reaching the telescope is maximal. Moreover, it is also clear that with the exception of Pixel 1, for each pixel in the row there is a value of the beam inclination angle for which it receives a maximum number of photons, and that this angle decreases with increasing position of the pixel in the row. This is, to a large extent quite normal, since according to the geometry in Fig. 3, as the angle δ increases, more and more of the light beam will enter the FoV of Pixel 1, while at the same time less and less of the same beam will remain in the FoV of the other pixels.

It should be noted however that the difference between the angle for which the total number of photons received by the detector is maximal and the angle for which the number of photons on received by Pixel 16 is maximal is quite small, of the order of 3°, suggesting that in practice it will be quite difficult to tune the inclination angle in order to optimize the calibration setup.

The conclusion of this analysis is straightforward. There is indeed a calibration beam inclination angle for which either the detector or its individual pixels can receive a maximal number of photons, but it is not clear at this time which should be the optimal configuration of choice and more work is necessary in order to elucidate this aspect.

4. SUMMARY AND CONCLUSIONS

The work in the present paper has been focused on the analysis of a ground-based light beam system to be used for the calibration of orbital UV telescopes such as the TUS, KLYPVE and JEM-EUSO telescopes. For this purpose, we have developed a custom software package, namely the GBSatCal package, which can be used for the analysis of the calibration systems for all three missions mentioned previously. Here, we have used it for the analysis of the ground calibration system of the TUS telescope, which is the simplest of the three.

One of the most important conclusions of the analysis is that while one can draw on the experience and technology developed for calibrating the UV telescopes of the PAO experiment, *i.e.* on the use of lasers, there is a simpler and more economically feasible alternative relying on the use of superbright LEDs which has been proposed by the authors of the present paper and which works equally well.

A second important conclusion of the present work is that the calibration geometry can be optimized, in the sense that our analysis has shown that for certain values of the angle made by the calibration light beam with the local horizontal, either the total number of photons reaching the detector is maximal, or that reaching an individual pixel. It is not clear, however, which is the best choice for optimizing the calibration procedure, and more work has to be done on this issue.

In terms of plans for future work, in the first place we will continue to work on the optimization of the calibration procedure, along the lines mentioned above. Secondly, we intend to further improve the GBSatCal software package by adding more up-to-date atmospheric models, such as the NRLMSISE00. Finally, we intend to start developing an LED pixelated calibration source along the lines discussed in Section 3, and we intend to report on our progress in a further publication.

REFERENCES

1. V. I. Abrashkin *et al*., IJMP **A 20**, *29*, 6865–6868 (2005).
2. B. A. Khrenov *et al*., AIP Conference Proceedings **566**, 57–75 (2001).
3. Santangelo *et al*., *Status of the JEM-EUSO Mission*, icrc2013-0738, 33rd International Cosmic Ray Conference, Rio de Janeiro, 2013.
4. Fick *et al*., JINST **1**, P11003 (2006).
5. J. Abraham *et al*., NIMPR **A 523**, 50–95 (2004).
6. The COSPAR International Reference Atmosphere (CIRA-2012), Ch. 1–3, Version 1.0, released 31.07.2012 (http://spaceweather.usu.edu/htm/cira).
7. The Hamamatsu R1463 PMT, http://www.hamamatsu.com/jp/en/R1463.html.
8. US Standard Atmosphere 1976, NASA Technical Report TM-X-74335, 1976 (http://ntrs.nasa.gov/archive/nasa/casi.ntrs.nasa.gov/19770009539.pdf).
9. Rees, Adv. Sp. Res. (COSPAR), **8**, *5–6* (1988).
10. J. M. Picone *et al*., J. Geophys. Res. **107**, *A12*, 1468 (2002).
11. The NASA Marshall Space Flight Center Earth Global Reference Atmospheric Model – 2010 Version, NASA Technical Report TM-2011-216467 (1976); http://ntrs.nasa.gov/archive/nasa/casi.ntrs.nasa.gov/20110012696.pdf.
12. Berat *et al*., Astroparticle Physics **33**, *4*, 221–247 (2010).
13. C. F. Bohren, D. R. Huffman, *Absorption and Scattering of Light by Small Particles*, Wiley-VCH Verlag GmbH & Co. KGaA, Weinheim, 2004.
14. Montanet, Report EUSO-SIM-REP-009-1.2 (2004).
15. V. Dimitriev *et al*., AIP Conf. Proc. **1118**, 116 (2009).
16. LEDEngin LZ1-00UV00, http://www.ledengin.com/files/products/LZ1/LZ1-00UV00.pdf.